remote sensing

MDPI

Technical Note

An Aftershock Deletion Method Based on Fault Buffer Zone

Guangliang Yang [1,2,*], Bingjie Zhao [3] and Yijun Liu [1]

[1] Key Laboratory of Earthquake Geodesy, Institute of Seismology, China Earthquake Administration, Wuhan 430071, China
[2] Institute of Disaster Prevention, Langfang 065201, China
[3] Zachry Department of Civil and Environmental Engineering, Texas A&M University, College Station, TX 77843, USA
* Correspondence: vfory@aliyun.com; Tel.: +86-180-8600-8898

Abstract: The existence of aftershocks in an earthquake sequence can impact the analysis of the mainshock. In this study, we present a method for deleting an aftershock sequence based on the spatial relationship between earthquakes and faults. This method improves the performance of space window selection in the classical K-K method by eliminating aftershocks with an ideal fault buffer zone. The determination of fault buffer zones is based on a trial-and-error analysis of 69,714 earthquake records from the China Seismic Network Center (CENC) collected between 1980 and 2020. We selected 20 typical big earthquakes (M_L7.0–8.0 or ~Ms6.6–8.0; for earthquakes above magnitude Ms7 or M_L7.2, M_L is approximately equal to Ms) as the mainshocks to establish the fault buffer zones. We also propose an empirical formula to determine the distance of the fault buffer zone by counting the aftershock deletion effect at different buffer distances. Compared with the classical K-K method, our method considers the correlation between the spatial distribution of aftershocks and faults, eliminates earthquake groups that are not related to the mainshock, greatly reduces the spatial range of aftershocks, improves the performance of deleting aftershocks of different magnitudes, and provides a new rule and reference for aftershock deletion.

Keywords: aftershock deletion; mainshock; fault buffer zone; K-K method

Citation: Yang, G.; Zhao, B.; Liu, Y. An Aftershock Deletion Method Based on Fault Buffer Zone. *Remote Sens.* **2023**, *15*, 1662. https://doi.org/10.3390/rs15061662

Academic Editor: Fumio Yamazaki

Received: 7 January 2023
Revised: 16 March 2023
Accepted: 16 March 2023
Published: 19 March 2023

1. Introduction

Earthquakes are one of the natural disasters that have a significant impact on life and property [1,2] and are often viewed as independent events. Earthquakes' statistical characteristics have always been an important tool for researchers to predict earthquakes and evaluate earthquake risk. Aftershocks are responses to stress changes produced by large earthquakes and represent the most common phenomenon triggered by earthquakes [3]. Aftershock analysis is important for the probabilistic seismic hazard analysis (PSHA) [4,5], as it involves a series of earthquakes that occur after the main earthquake. After the mainshock, the stress distribution of the fault changes significantly, resulting in a series of aftershocks with the process of stress readjustment. According to Shilen and Toksoz [6], aftershocks are entirely inconsistent with the Poisson process, and they can obscure the statistical characteristics of an earthquake as an independent event to some extent [7], such as the unknown recurrence period [8]. Although the impact of aftershocks on the recurrence cycle is small, it cannot be ignored when evaluating local earthquake risk [6]. Therefore, deleting aftershocks is crucial for earthquake statistical analysis and earthquake prediction.

Numerous studies have been conducted to develop effective and efficient methods for removing aftershocks. Knopoff and Gardner [9] deleted aftershocks by eliminating all earthquake sequences within a particular distance and time period of a large earthquake event within a square area. Shlien and Toksdz [10] considered the spatial distance, time interval, and regional seismic activity to determine the mainshock-aftershock relationship between two earthquake events. Console et al. [11] used an empirical formula that factors

in the spatial distance and magnitudes of two earthquake events to remove aftershocks. The K-K method, proposed by Keilis-Borok and Knopoff L et al. [12], adjusts the size of the spatial and time window used to remove aftershocks based on the magnitude of the mainshock. Davis and Cliff [13] presented a unified relationship between earthquakes and the parameters of the space-time window, while Chen et al. [8] determined aftershocks by considering the length of the fault and the time window specified by Console et al. [11]. In recent years, some other methods have also been proposed, such as stochastic decluttering based on point processes [14], nearest-neighbor distances of events in the space-time-energy domain [15–17], narrow spatial aftershock zones [18], and nonparametric network-tree aftershock identification [19]. Most of these methods are based on temporal and spatial relations and can quickly remove aftershocks from the entire earthquake catalog.

The methods mentioned above typically use circular or square areas centered on the main earthquake's epicenter to determine the spatial range of aftershocks, without considering the fault characteristics closely related to earthquakes. However, aftershocks usually occur on the same fracture plane as the mainshock, and stress changes resulting from Coulomb stress transfer can also trigger aftershocks in other fault zones. Stress drops and normalized rupture width most strongly correlate with aftershock productivity [20–23]. Nevertheless, most earthquakes are concentrated around the fault zone near the mainshock's epicenter. It is important to note that earthquakes are the result of tectonic movements, which release the accumulated high stress in the crust through fault movements. Faults are a macroscopic feature of tectonic movements, and the occurrence of earthquakes is highly correlated with the fault scale, including secondary faults, faults, plane width, and fault types, especially its length. The fault length of an active fault is positively correlated with the stress accumulation in the crust.

The spatial location of earthquakes is closely related to fault zones. To reduce the spatial range of aftershocks selected by the K-K method, a new quick method called the "fault buffer zone" is proposed. This method is mainly based on the positive correlation between the crustal stress and the fault length. As a quick method, it temporarily ignores other attributes of the fault, such as fault dislocation mode and fault plane, which require careful geological verification. The basic idea is to select the closest related fault of a specific mainshock as the main fault and use the line elements determined by the main fault to extend a certain distance outward to determine the buffer zone of the main fault, which is the aftershock space. Fault length is a comprehensive response to geological structure and stress accumulation. Therefore, this method considers the correlation between aftershocks, main faults, and differences in geological tectonic environments in different regions.

The introductory section of this paper provides an overview of the fault buffer zone method for deleting aftershocks. The subsequent section describes the methodology for determining the main parameters of the fault buffer zone method. The third section presents the empirical formula for calculating the fault buffer zone, which is based on a statistical analysis of earthquakes in the Chinese mainland since 1980 and tests on major earthquakes. The final section summarizes the main conclusions of the study.

2. Aftershock Deletion Algorithm Based on "Fault Buffer Zone"

The K-K algorithm [12] employs an empirical method to remove aftershocks by defining a spatial and temporal based on the magnitude of the mainshock. The mainshock magnitude is denoted as M, the aftershock magnitude as m, the distance between two earthquakes as r, the time interval as Δt, the spatial window distance as R_0, and the time window interval as T_0. If the following condition is met, then m is classified as the aftershock of M:

$$r \leq R_0(M);\ \Delta t \leq T_0(M);\ m < M, \tag{1}$$

The empirical value of the aftershock space and time window of the K-K algorithm is presented in Table 1.

Table 1. Aftershock space and time window of the K-K method.

M	$R_0(M)$/km	$T_0(M)$/d	M	$R_0(M)$/km	$T_0(M)$/d
2.0–2.5	30	6	5.0–5.5	50	183
2.5–3.5	30	12	5.5–6.5	50	365
3.5–4.0	40	23	6.5–7.0	100	548
4.0–4.5	40	46	7.0–7.5	100	730
4.5–5.0	40	92	7.5–8.0	150	913

The K-K method's spatial window is typically a circle centered on the epicenter. In this study, we replace the circle with a "fault buffer zone" that considers the correlation between earthquakes and their corresponding seismogenic faults. The fault buffer zone is a closed polygon that extends a certain distance outward from the seismogenic fault. Figure 1 shows the flowchart of the aftershock deletion algorithm based on a fault buffer zone.

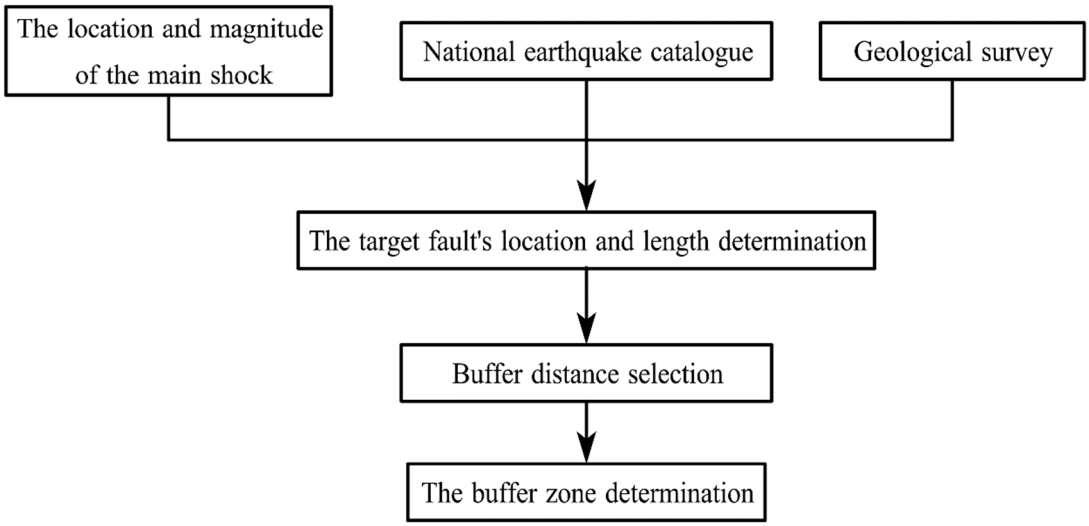

Figure 1. Flow chart of aftershock deletion algorithm based on the fault buffer zone.

Figure 1 illustrates the aftershock deletion algorithm based on the fault buffer zone. The seismogenic fault determined by geological survey or focal mechanism solution and closest to the epicenter of the mainshock is considered the target active fault and is simplified into a linear unit. Active faults are those that have been active since the late Quaternary and may still be active today or be reactivated in the future. The proposed method for aftershock deletion only requires the identification of faults and the determination of their existence through the analysis and interpretation of aerial and satellite photos, geophysical maps, and geological maps, without considering fault type. This is because the aftershocks are distributed in the buffer zone, which is established with the seismogenic fault as the center, regardless of the fault type, including normal fault, reverse fault, and strike-slip fault.

The fault buffer zone replaces the circular spatial window of the K-K method by extending a certain distance outward from the seismogenic fault, which is simplified into a linear unit, to form a closed polygon.

This aftershock deletion algorithm based on the fault buffer zone requires determining the following parameters for the earthquake (mainshock) being studied:

(1) The seismogenic fault closest to the mainshock was identified through a geological survey or focal mechanism solution, simplified into a linear unit.
(2) The length of the seismogenic fault.
(3) The buffer distance of the fault buffer zone.

2.1. Determining the Seismogenic Fault and Its Length Related to the Mainshock

Earthquakes may be associated with a single fault, multiple faults, multisegmented faults, or concealed faults [24]. To identify the seismogenic fault related to the mainshock, postearthquake investigation and focal mechanism solutions can be used. If the earthquake is related to multiple faults, the faults can be simplified into a linear unit. The next step is to determine the length of the seismogenic fault. The empirical Formula (2) by Guo et al. [25] shows the relationship between earthquake magnitude (surface wave magnitude) and fault length, while Wells and Coppersmith [26] proposed a formula relating earthquake moment magnitude (Mw) and fault rupture length. However, China's earthquake catalog uses near earthquake magnitude to define the magnitude (M_L) in the early stage. In this paper, we still use the calculation formula of M_L and fracture length, because China earthquakes catalog with M magnitude by default and will introduce deviation if historical earthquakes are converted to Mw magnitude and it is not possible to use Mw for small earthquakes. For earthquakes above magnitude Ms7.0 or M_L7.2, M_L is approximately equal to Ms. In this formula, M represents the earthquake magnitude, and L represents the length of the fault in kilometers. There is a significant positive correlation between the logarithm of earthquake magnitude and fault length.

$$M = 3.3 + 2.1\log L, \tag{2}$$

2.2. Determination of Fault Buffer Distance

Based on the aforementioned methodology, the fault buffer zone is determined by taking the seismogenic fault as the center and extending a certain distance, which is determined by the Joyner-Boore distance. The Joyner-Boore distance refers to the shortest distance from an observation point on the ground to the projection of the fault on the ground. The size of the buffer zone is determined by the magnitude of the mainshock. A larger magnitude corresponds to a larger Joyner-Boore distance and a larger buffer zone.

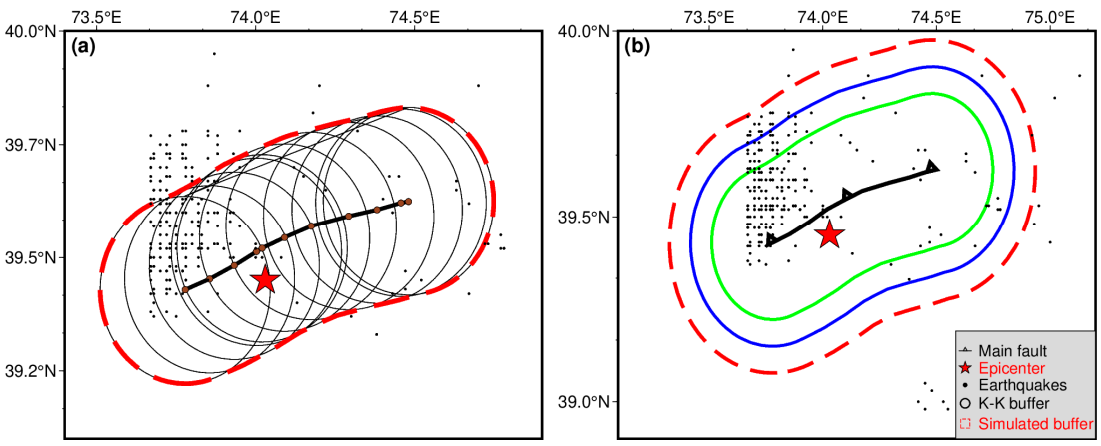

Figure 2. Method for establishing and adjusting the fault buffer zone (The red five-pointed star represents the main earthquake, while the black line represents its corresponding seismogenic fault. The black line on the left of the figure above represents the seismogenic fault. The circles represent the buffer range of each point on the fault, and the red envelope represents the buffer area of the fault. The multiple envelope areas on the right of the figure above represent different buffer areas corresponding to different earthquakes). (**a**) The buffer distance for a earthquake; (**b**) adjustment of the buffer distance.

There are 69,714 earthquake records of magnitude greater than M_L3.0 collected from the China Seismic Network Center (CENC) between 1980 and 2020. While strong earthquakes generally receive great attention and provide rich observation data, such as seismogenic faults, focal mechanism solutions, and geological observations, it is important to find an appropriate fault buffer distance for earthquakes of different magnitudes. To accomplish

this, we selected almost all 20 typical strong earthquakes with magnitudes ranging from M_L7.0–M_L8.0(∼Ms6.6–8.0) as the main shocks and carried out trial-and-error analysis. The time and space windows provided by the K-K method were used as a reference to determine the initial value of the spatial location and length of the main faults.

To determine the appropriate buffer distance for earthquakes of different magnitudes, we adjusted the buffer distance, i.e., the Joyner-Boore distance, according to the magnitude of the earthquake (Figure 2), with the initial value set to the space window distance R_0 of the K-K method. Proper adjustment of the buffer distance is necessary to effectively handle the aftershocks of strong earthquakes.

3. Statistical Results and Discussion

The trial-and-error analysis of aftershock deletion is carried out using earthquake catalog data (69,714 events greater than M_L3.0) collected by CENC from 1 January 1980 to 23 December 2020. Among them, there are 2772 earthquakes with magnitudes greater than or equal to 5.0 and 461 earthquakes with magnitudes of 6.0 and above. The fault data used in this analysis is sourced from the active tectonic map of China (1:4 million) developed by Academician Deng Qidong [27] and provided by the National Seismological Science Data Center. The fault data includes the geographical location and fault attributes of major faults in China, such as fault name, length, strike, dip, dip angle, fault nature, and the latest active age.

In Section 2, we used the fault buffer zone method to analyze the typical aftershocks of Ms7.0~8.0 earthquakes. We obtained appropriate buffer distances for 20 great earthquakes with magnitudes between 7.0 and 8.0. These earthquakes were divided into six groups according to their magnitudes: M_L7.0, M_L7.1, M_L7.2, M_L7.4, M_L7.6, and M_L8.0 (for earthquakes above magnitude Ms7.0 or M_L7.2, M_L is approximately equal to Ms). The relationship between an earthquake's magnitude and fault buffer distance was obtained for each group using least square error.

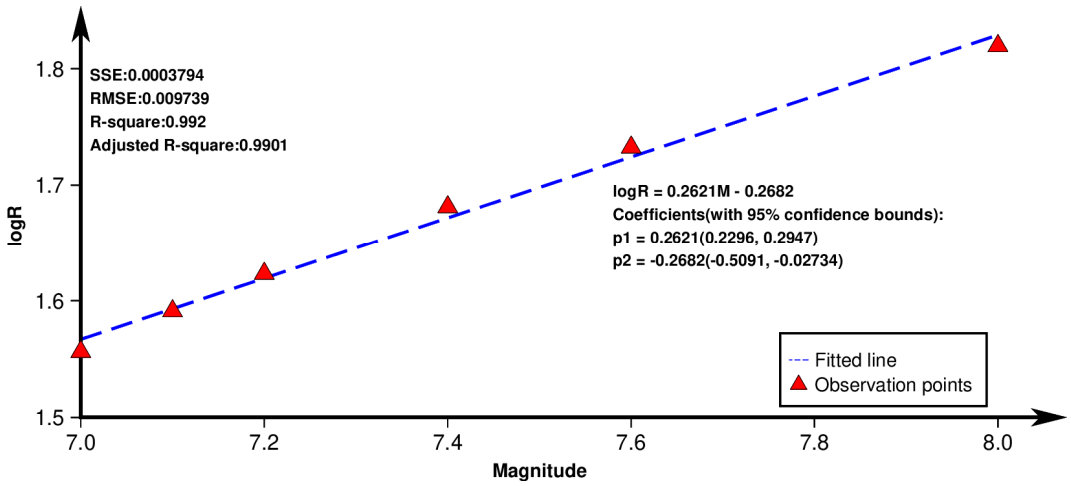

Figure 3. Illustrates the logarithmic relationship between the magnitude and the fault buffer distance (The red triangle indicates the statistical optimal fracture buffer distance, while the blue dotted line represents the fitted trend of fault buffer distance. The fitting correlation coefficient is shown in the figure, with the SSE and RMSE being very low, and the R-square value reaching 0.99; SSE: sum of squares of residuals; RMSE: root mean square error; R-square: coefficient of determination).

To examine the relationship between the magnitude of the mainshock and buffer distance, and to test its effectiveness in deleting aftershocks for earthquakes of other magnitudes, we fitted a function between the magnitude and the buffer distance (Figure 3) and analyzed the results in Formula (3). The fitting effect was excellent, with a low SSE (sum of squares of residuals), a low RMSE (root mean square error), and a coefficient of determination (R-square) of 0.99. In Section 3.1, we provide a detailed statistical analysis

of aftershock deletion for mainshocks of different magnitudes, including M_L7.0, M_L7.1, M_L7.2, M_L7.4, M_L7.6, and M_L8.0.

$$\log R = 0.2621M - 0.2682, \quad (3)$$

3.1. Verification of M_L 7.0~M_L7.1 Earthquake Fault Buffer Zone

Table 2 shows the M_L7.0~7.1 earthquakes that occurred in mainland China since 1980. There was a total of six earthquakes, and the fault buffer zone calculated according to Formula (3) for each earthquake is shown in the table. These buffer zones can be used for aftershock deletion in future earthquakes with similar magnitudes.

Table 2. Fault buffer distance of the M_L7.0 and M_L7.1 earthquakes.

ID	M_L	Date	Location			Target Fault	Buffer Distance (km)
			Longitude	Latitude	Depth		
a	7.0	25 November 2016	74.1°	39.2°	10	Muji fault	36
b	7.1	5 November 1988	90.7°	32.9°	/	Chibu zhangcuo-zhasa fault	39
c	7.1	26 April 1990	100.13°	36.12°	29	Northern margin fault of Gonghe basin	39
d	7.1	5 October 2008	74.03°	39.45°	10	Kazikearte fault	39
e	7.1	7 October 2014	100.55°	23.4°	10	Sanlinyang-siyongjie fault	39
f	7.1	18 November 2017	95°	29.75°	10	Ani bridge fault	39

Figure 4 illustrates the distribution of aftershocks and target active faults of the M_L7.0 and M_L7.1($\sim$*Ms*6.6–*Ms*6.9) earthquakes. The red dashed area represents the fault buffer zone calculated using Formula (3), while the black circular area denotes the spatial range of the deleted aftershocks selected by the K-K method corresponding to the mainshock. In Figure 4a, the fault buffer of a shallow strike-slip M_L7.0 earthquake near the western end of the Muji graben basin in the northern part of the Pamir syntax [28] is shown. The buffer distance, which is equal to 36 km, is obtained by applying Formula (3). The number of aftershocks falls within the K-K method prediction, with aftershocks mainly between M_L3.0 and M_L4.8. The number of aftershocks decreases year by year, and the focal depth ranges from 4 to 16 km.

On the other hand, Figure 4b–f show the fault buffer zone of several M_L7.1 earthquakes, with a calculated distance of 39 km using Formula (3). The dotted red line represents the buffer zone, which basically captures the aftershock distribution range. Aftershock magnitudes are generally small, concentrated in M_L3.0–4.0.

The figure demonstrates that the distribution of aftershocks determined by the fault buffer zone generally conforms to the structural geological distribution. In Figure 4b, a strike-slip fault with a slight overthrust component [29] occurred between the southwest of Qinghai Province and the edge of the Tuotuo River. The aftershocks are mainly concentrated in the area near the fault. The mainshock (shown in Figure 4c) occurred near the Tanggemu Farm on the southwestern edge of the Gonghe Graben Basin, Qinghai, and the magnitude of aftershocks ranges from M_L3.0 to M_L4.0. The aftershocks in Figure 4d mainly occur at the junction of China, Tajikistan, and Kyrgyzstan, with a broad range of magnitudes from M_L3.0 to M_L6.4 [30]. The mainshock in Figure 4e occurred in Jinggu, Yunnan, with its epicenter located at the junction of various subduction, collision, suture, overlap, and strong crustal accretion [31]. The magnitude of aftershocks is mostly M_L3.0–4.0. The aftershocks in Figure 4f are located around the mainshock and extended along the northwest and southeast sides of the mainshock [32], with the largest aftershock magnitude being M_L5.6.

In summary, the fault buffer distance of 39 km is appropriate for M_L7.0–M_L7.1 earthquakes. As shown in Figure 4, the aftershocks within the fault buffer zone are more concentrated and better reflect the correlation between the aftershock sequence and fault strike compared to the aftershocks filtered out by the K-K method.

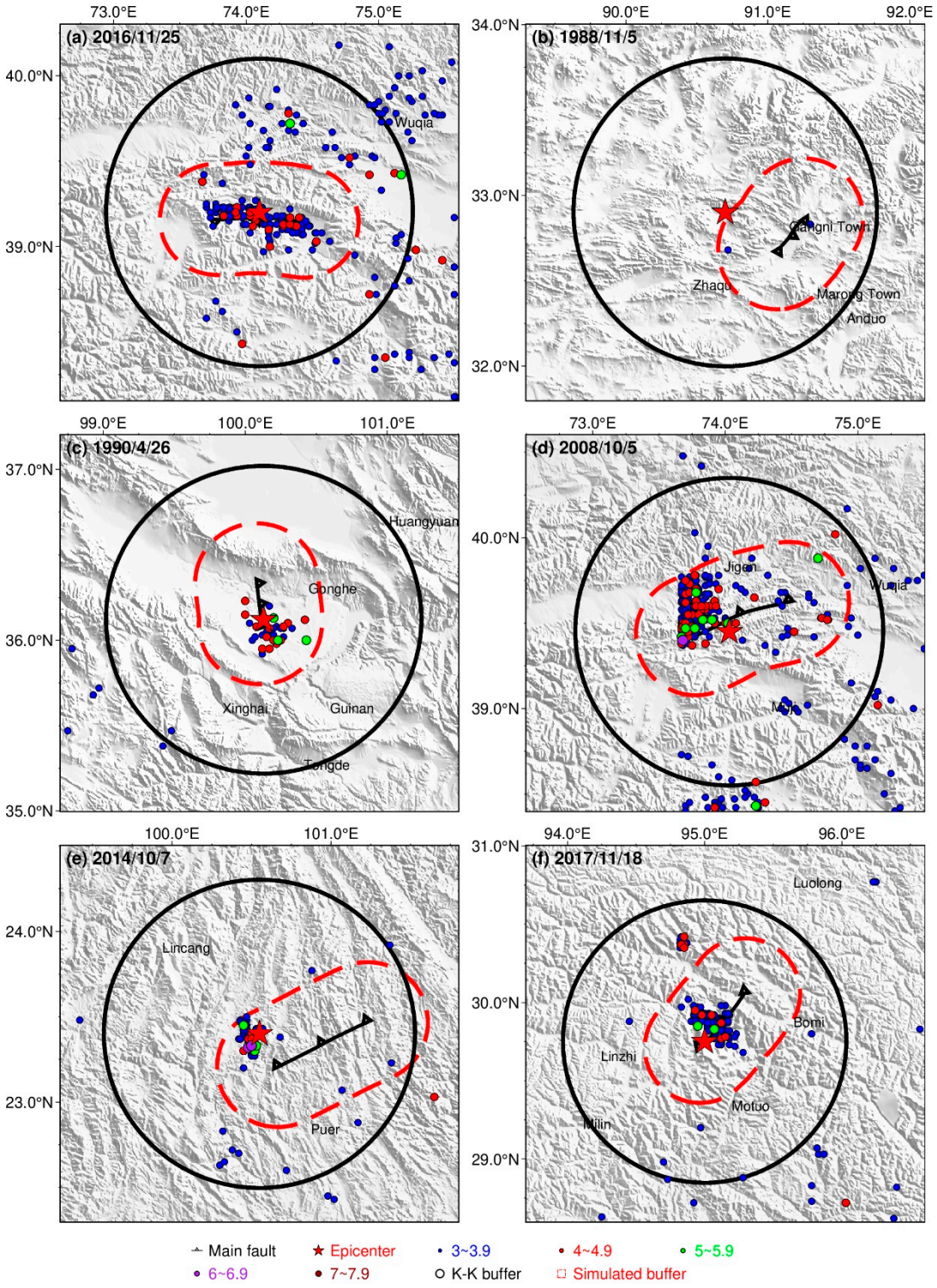

Figure 4. The fault buffer zone of $M_L7.0$ and $M_L7.1$ earthquakes, as well as the distribution of aftershocks (the red dotted line indicates the fault buffer zone, while the black circle indicates the range of K-K aftershocks; the red five-pointed star represents the mainshock; and the time of the mainshock is displayed in the upper left corner of the figure; the legend in the lower right corner of the figure explains the symbols used in the figure). (**a**) The Aktau $M_L7.0(Ms\,6.7)$ earthquake; (**b**) the Xiji and toto river $M_L7.1(Ms\,6.8)$ earthquake; (**c**) the Tanggemu $M_L7.1(Ms\,6.9)$ earthquake; (**d**) the Wuqia $M_L7.1(Ms\,6.8)$ earthquake; (**e**) the Jinggu $M_L7.1(Ms\,6.6)$ earthquake; (**f**) the Linzhi $M_L7.1(Ms\,6.9)$ earthquake.

3.2. Verification of M_L7.2 Earthquake Fault Buffer Zone

Table 3 displays the M_L7.2 earthquakes that have occurred in mainland China since 1980, with a total of six earthquakes selected for the statistics of aftershock deletion, using them as the mainshock.

Table 3. Fault buffer distance of M_L7.2 earthquake.

ID	M_L	Date	Location			Target Fault	Buffer Distance (km)
			Lon	Lat	Depth		
a	7.2	24 January 1981	101.17°	31°	12	Xianshuihe fault	42
b	7.2	3 February 1996	100.22°	27.3°	10	Lijiang-Daju fault	42
c	7.2	19 November 1996	78.35°	35.43°	/	Eslak karaur	42
d	7.2	25 August 2008	83.65°	30.93°	10	Yare fault	42
e	7.2	20 April 2013	102.98°	30.3°	17	Guanxian-Jiangyou fault	42
f	7.2	8 August 2017	95°	29.75°	10	Tazang fault	42

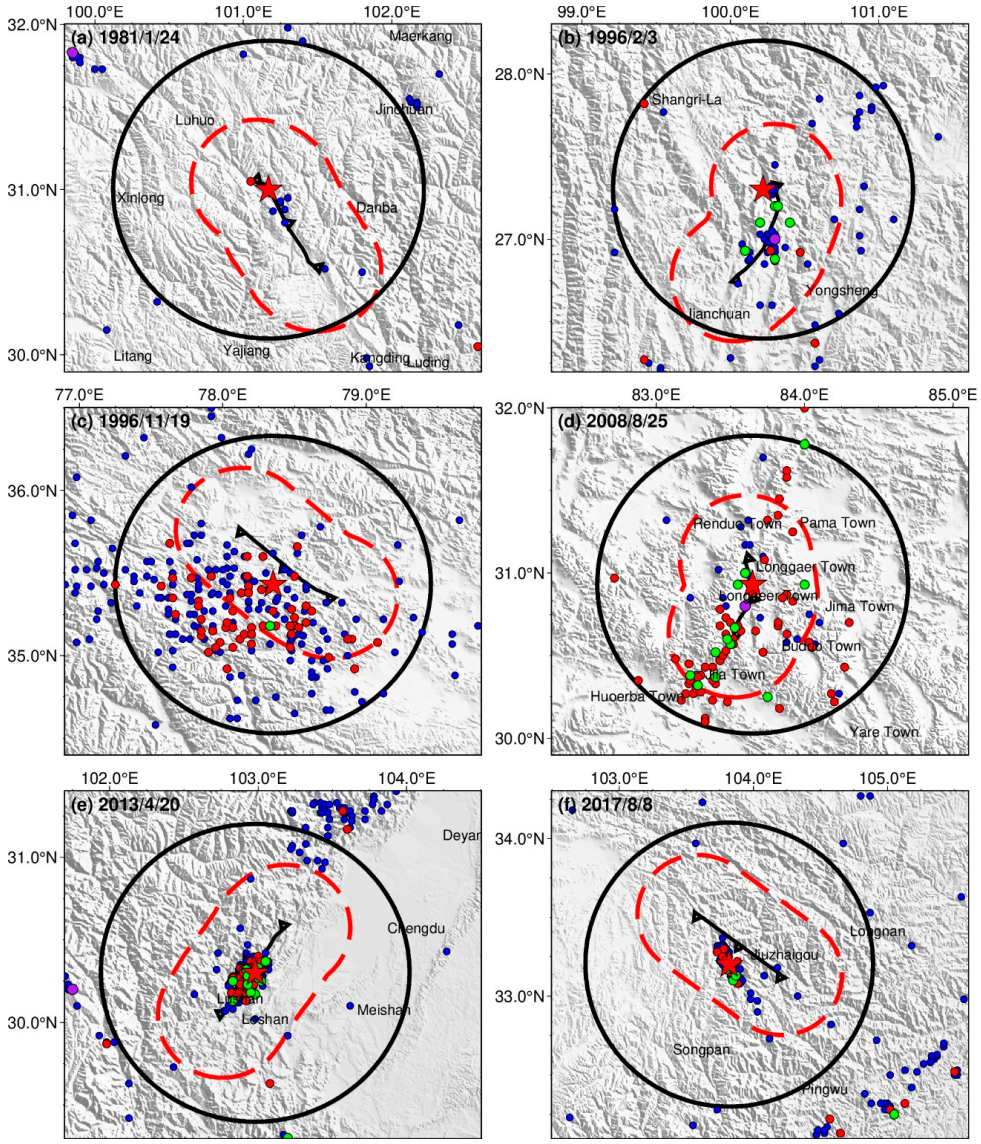

Figure 5. Establishment of M_L7.2 earthquake fault buffer zone. (**a**) The Daofu M_L7.2(Ms6.8) earthquake; (**b**) the Lijiang M_L7.2(Ms7.0) earthquake; (**c**) the Hetian M_L7.2(Ms7.1) earthquake; (**d**) the Zhongba M_L7.2(Ms6.8) earthquake; (**e**) the Lushan M_L7.2(Ms7.0) earthquake; (**f**) the Jiuzhaigou M_L7.2(Ms7.0).

According to Formula (3), the fault buffer distance of 42 km is suitable for removing aftershocks from all the M_L7.2 earthquakes. The aftershocks of the Daofu earthquake, in Sichuan Province, shown in Figure 5a, are distributed on the northwest strip and have generally small magnitudes and shallow focal depths, except for a few earthquakes. The mainshock in Figure 5b occurred at the Lijiang-Daju fault, which is a normal fault with a left-handed movement component, and the aftershocks are distributed in the north-south direction, with the maximum aftershock magnitude of 6.3. The mainshock in Figure 5c occurred in the Karakoram Pass southwest of Hotan, Xinjiang. Most aftershocks are distributed in the southwest of the mainshock with a low magnitude, and the earthquake distribution shows no obvious characteristics [33]. The lack of earthquake data may be the reason for this, as it is in the border area between two countries, some earthquakes may not have been recorded.

The mainshock in Figure 5d occurred in Zhongba, Tibet, with a generally small aftershock magnitude. The mainshock in Figure 5e occurred in Lushan County, Yaan City, Sichuan Province, which is similar in focal nature to the Wenchuan earthquake (in 2008). In Figure 5f, the mainshock occurred in Jiuzhaigou County, Aba Tibetan Autonomous Prefecture, and the northern Sichuan Province. The aftershocks of this earthquake are characterized by a small number of moderate and strong aftershocks and a large difference in magnitude between the largest aftershock and the mainshock. The sequence of aftershocks showed a NW-SE trend [34].

3.3. Verification of M_L 7.4(Ms7.4) Earthquake Fault Buffer Zone

Table 4 shows four mainshocks with a magnitude of M_L7.4, all of which occurred in Western China.

Table 4. Fault buffer distance of M_L7.4 earthquake.

ID	M_L	Date	Location			Main Fault	Buffer Distance (km)
			Lon	Lat	Depth		
a	7.4	23 August 1985	75.6°	39.58°	/	Kazikealte fault	48
b	7.4	21 March 2008	81.43°	35.8°	/	Altun Mountain's south margin fault	48
c	7.4	14 April 2010	96.58°	33.22°	14	Ganzi-Yushu-Fenghuoshan	48
d	7.4	12 February 2014	82.52°	36.13°	10	Yare fault	48

The fault buffer distance of 48 km is suitable for all mainshocks. The mainshock in Figure 6a happened in Wuqia County, Xinjiang Uygur Autonomous Region. The mainshock in Figure 6b is close to the Kunlun Mountain Watershed at the junction of Yutian, Cele, and Tibet. This earthquake is believed to have been caused by a tensile rupture with a strike-slip component of the Guozhacuo fault of the Altyn Tagh fault zone under the action of the NS direction force [30], and the aftershock sequence attenuates quickly, mainly in Tibet, Ritu, and parts of Xinjiang. The mainshock in Figure 6c occurred in Yushu, Qinghai Province, and the largest aftershock magnitude is M_L6.6. The region with the most concentrated aftershocks is located west of the mainshock, and the spatial distribution of aftershocks gradually shrank westward over time [35]. The mainshock in Figure 6d occurred in Yutian, Xinjiang, and its aftershocks are distributed in a southwest direction and spread along one side of the fault.

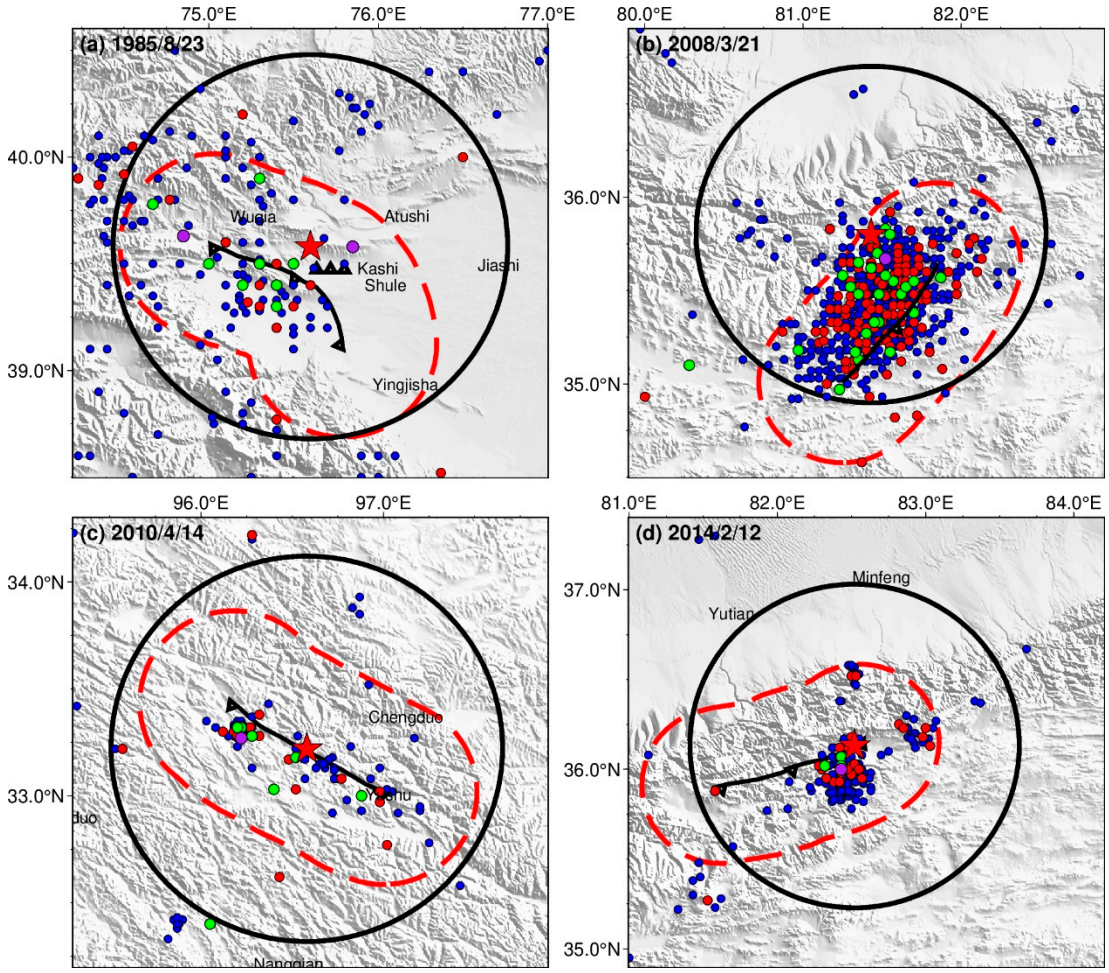

Figure 6. Establishment of M_L7.4 earthquake fault buffer zone. (**a**) The Wuqia M_L7.4(Ms7.4) earthquake; (**b**) the Yutian M_L7.4(Ms7.4) earthquake; (**c**) the Yushu M_L7.4(Ms7.1) earthquake; (**d**) the Yutian M_L7.3(Ms7.3) earthquake.

3.4. Verification of M_L 7.6(Ms7.6) Earthquake Fault Buffer Zone

There are two mainshocks with M_L7.6, and the fault buffer distance is 54 km (Table 5).

Table 5. Fault buffer distance of M_L7.6 earthquake.

ID	M_L	Date	Location			Target Fault	Buffer Distance (km)
			Lon	Lat	Depth		
a	7.6	18 November 1997	87.3°	35.2°	/	Altun Mountain's south margin fault	54
b	7.6	6 November 1988	99.72°	22.83°	13	longling-lancang fault	54

The mainshock in Figure 7a, which occurred in Mani, Tibet, has a buffer distance of 54 km. The aftershocks have small magnitudes, and the sequence decays faster with time. The mainshock in Figure 7b occurred in Lancang County, at the junction of Gengma and Cangyuan Counties in southwest Yunnan. The aftershocks are densely distributed along the Longling-Lancang fault, which includes the surrounding dense earthquake clusters. It was found that the maximum aftershock magnitude was 7.2. This earthquake can also be considered a double mainshock aftershock type.

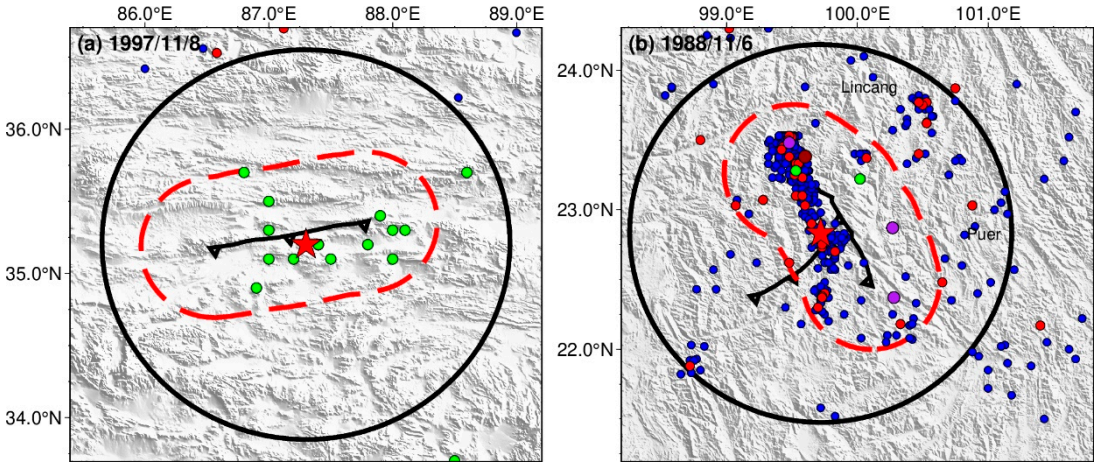

Figure 7. Establishment of M_L7.6) earthquake fault buffer zone. (**a**) the Mani M_L7.6(Ms7.9) earthquake. (**b**) the Lancang-gengma M_L7.6(Ms7.6) earthquake.

3.5. Verification of M_L 8.0(Ms8.0) Earthquake Fault Buffer Zone

Since 1980, there have been two earthquakes in mainland China with a magnitude greater than M_L8.0(Ms8.0). The first was the M_L8.1(Ms8.1) earthquake that occurred west of Kunlun Mountain Pass in 2001. The second was the Wenchuan earthquake on May 12, 2008, which caused many casualties. The Wenchuan earthquake occurred in Sichuan Province; its epicenter was at 103.4°E, 31°N, and had a focal depth of 14 km [36]. The main fault responsible for this earthquake is the Yingxiu-Beichuan fault [37].

Figure 8 shows the buffer distance of the M_L8.0 Wenchuan earthquake, which is 66 km. Aftershocks mainly occurred in areas near the mainshock, such as Wenchuan, Beichuan, Mianzhu and the number of aftershocks was large. However, the magnitude of aftershocks was generally small, and it decreased slowly over time. The aftershocks were densely distributed along the decreased direction of the mainshock.

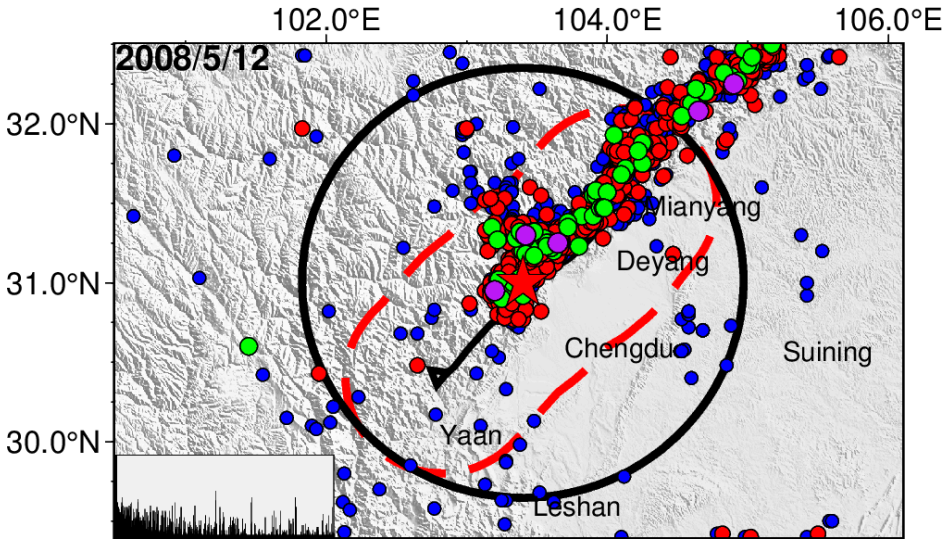

Figure 8. Establishment of M_L8.0(Ms8.0) earthquake fault buffer zone.

4. Test of Fault Buffer Zone of Mainshock and Discussion

Formula (3) was obtained using the trial-and-error method based on an earthquake with a magnitude range of M_L7.0–M_L8.0($\sim Ms$5.6–Ms8.0). Tests have shown that the improved algorithm, based on the fault buffer zone, is also suitable for different magnitudes,

such as $M_L8.1(Ms8.1)$, $M_L6.8((Ms6.6))$, and $M_L5.9(Ms5.6)$ (Table 6). The results of aftershocks selected by both methods are presented in Figures 9 and 10. When compared with the original K-K algorithm, the fault buffer zone method selects aftershocks that are clustered and centered on the target fault, which is consistent with the correlation between earthquake occurrence and geological structure. The earthquake shown in Figure 9a occurred in the west of the Kunlun Mountain Pass, and it is the largest earthquake in China in 70 years. Formula (3) was used to calculate the buffer distance, which was found to be 71.58 km. The earthquake shown in Figure 9b occurred in Xiaojin County, Aba Tibetan, and Qiang Autonomous Prefecture, Sichuan Province, with a buffer distance of 32.67 km. The earthquake in Figure 9c occurred in Hejing, Xinjiang, with a buffer distance of 18.98 km. Figure 9d is the aftershock deletion of Changning earthquake, Sichuan, China. The aftershock sequence has a low magnitude and a concentrated distribution, indicating that this method can accurately and quickly delete aftershocks, even for earthquakes with lower magnitudes. The three applications demonstrate that our method takes the fault strike into account. Figure 10 shows the precise location of the recent Changning earthquake in Sichuan and the range of deleted aftershocks using this algorithm. The figure shows that this algorithm can effectively distinguish between aftershocks of different mainshocks.

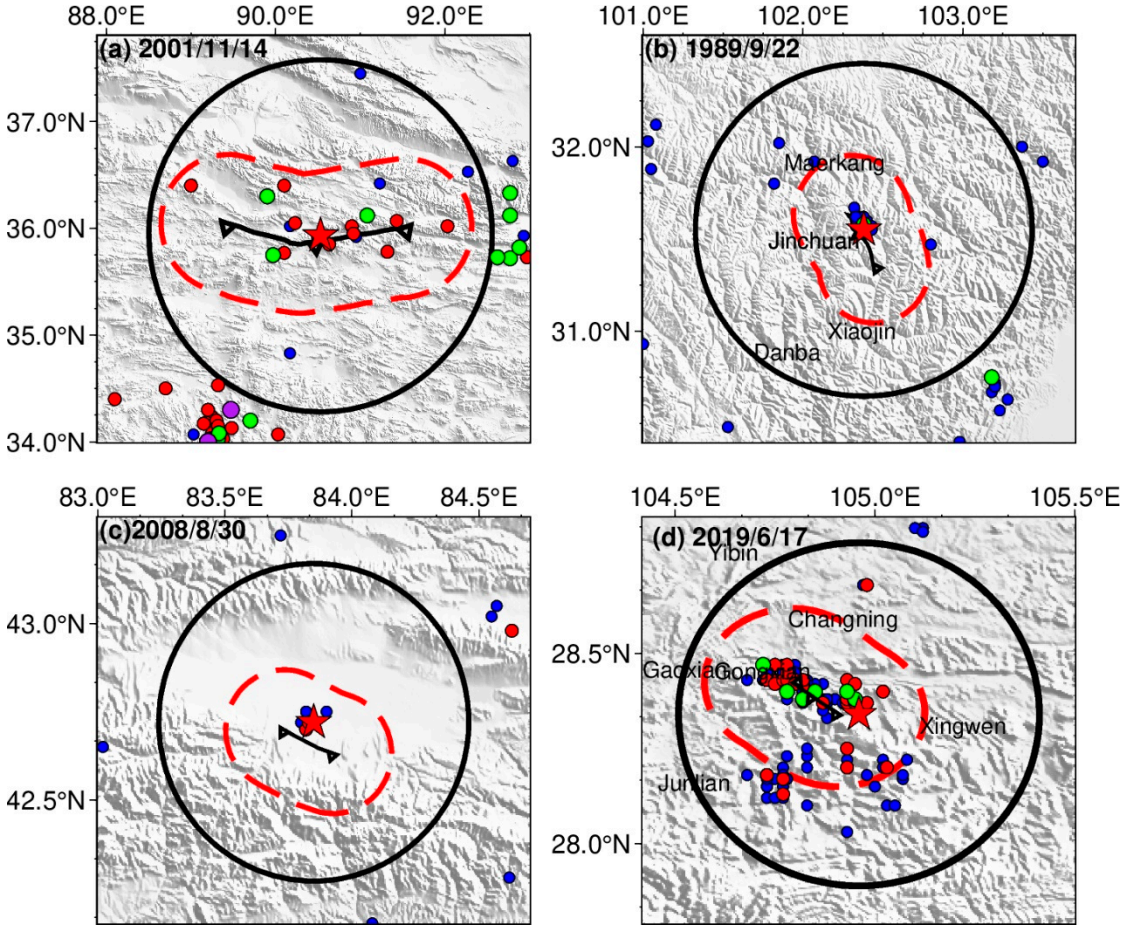

Figure 9. Establishment of three earthquakes' fault buffer zones in Table 6. (**a**) the Kunlun Mountain Pass $M_L8.1(Ms8.1)$ earthquake. (**b**) the Xiaojin $M_L6.8(Ms6.6)$ earthquake; (**c**) the Hejing $M_L5.9(Ms5.6)$ earthquake; (**d**) the Changning $M_L6.3(Ms6.0)$ earthquake.

Table 6. Fault buffer distance of other earthquakes.

ID	M_L	Date	Location			Target Fault	Interception Method
			Lon	Lat	Depth		
a	8.1	14 November 2001	90.53°	35.93°	10	Muziluk-Whale Lake	Far-end
b	6.8	22 September 1989	102.38°	31.55°	10	Malkang fault	Far-end
c	5.9	30 August 2008	83.85°	42.72°	6	Southern margin fault of Greater Yuludus Basin	Both sides
d	6.3	17 June 2019	104.97°	104.97°	16	104.97°	Far-end

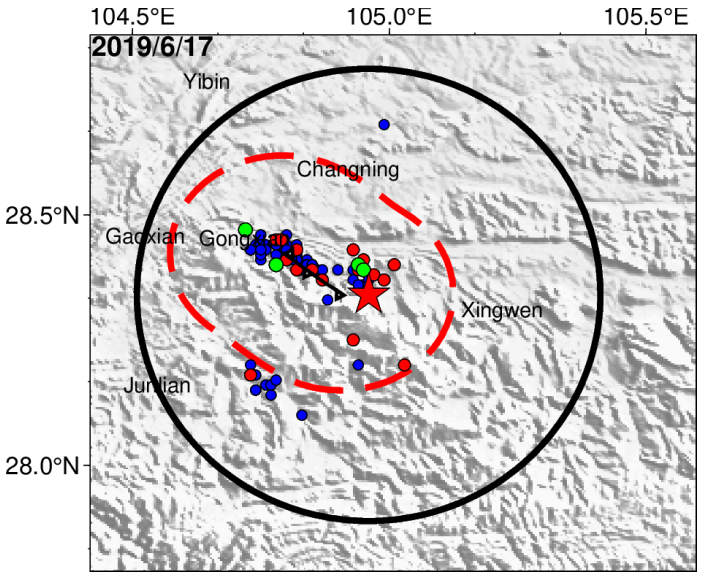

Figure 10. The aftershock deletion of Changning earthquake, Sichuan, China using the fault buffer zone algorithm.

The improved K-K aftershock deletion algorithm based on the fault buffer zone is more effective and accurate than the original K-K method. It selects aftershock sequences that are more concentrated and distributed along the effective faults, leading to a reduction in the number of aftershocks with time while the magnitude of the aftershocks is generally small. This approach is applicable to earthquakes above M_L6.3 and provides a more accurate aftershock sequence.

5. Conclusions

Removing aftershocks, that is, separating clustered events (i.e., aftershocks) from background earthquakes in the epicenter area. Accurately obtaining the aftershock of a mainshock can reveal changes in seismic activity in time and space [38]. Based on this, the accurate Coulomb stress and b value can be calculated, and the change characteristics of the fault stress and subsequent earthquake occurrence trend can be obtained.

In this paper, we propose a novel method for removing aftershocks based on the fault buffer zone. Our method builds on the basic assumption that there is a high correlation between earthquake magnitude and a seismogenic fault. Instead of using a circular area centered on the earthquake epicenter, our approach employs the fault buffer zone to accurately identify and remove aftershocks. The conclusions of this paper are as follows:

1. We conducted a statistical analysis of earthquakes with magnitudes of M_L7.0~8.0 in mainland China since 1980 and divided the 20 earthquakes into six groups for analysis, ranging from M_L7.0, M_L7.1, M_L7.2, M_L7.4, M_L7.6, and M_L8.0 (or $\sim Ms$6.6–8.0 and for earthquakes above magnitude Ms7 or M_L7.2, M_L is approximately equal to Ms). By using a trial-and-error method, we established an empirical formula for the fault buffer

distance. Our trials on the aftershock deletion of other magnitude earthquakes above M_L5.9 show that this empirical formula is also effective, and the deleted aftershock sequences are accurately clustered using the fault buffer zone-based spatial window method. We compared our method with the K-K method and found that our method is applicable for deleting aftershocks at different magnitudes.

2. The test results show that the proposed fault buffer zone-based method improves on the traditional K-K method by taking into account relationships between earthquake magnitude and fault rupture length, increasing the accuracy of aftershock selection. The results of aftershock deletion using this method show good agreement with the actual earthquake occurrence distribution.

However, this method still has room for improvement, as the presence of a concealed fault may affect the accuracy of aftershock deletion. Furthermore, it is necessary to verify the applicability of the empirical formula in other regions of the world.

Author Contributions: Conceptualization, G.Y. and B.Z.; methodology, G.Y.; statistical analysis, Y.L.; validation, G.Y., Y.L. and B.Z.; formal analysis, G.Y.; writing—original draft preparation, G.Y. and Y.L.; writing—review and editing, G.Y. and B.Z.; visualization, Y.L.; supervision, G.Y. All authors have read and agreed to the published version of the manuscript.

Funding: This research was funded by the National Natural Science Foundation of China (grant No. 42174104, U1939204, and 41204014) and Hubei provincial Natural Science Foundation of China (2022CFB350).

Data Availability Statement: Not applicable.

Acknowledgments: The authors thank the editors and the anonymous reviewers for their comments and constructive suggestions.

Conflicts of Interest: The authors declare no conflict of interest. The funders had no role in the design of the study; in the collection, analyses, or interpretation of data; in the writing of the manuscript, or in the decision to publish the results.

References

1. Chaudhary, M.T.; Piracha, A. Natural Disasters—Origins, Impacts, Management. *Encyclopedia* **2021**, *1*, 1101–1131. [CrossRef]
2. Kamranzad, F.; Memarian, H.; Zare, M. Earthquake Risk Assessment for Tehran, Iran. *ISPRS Int. J. Geoinf.* **2020**, *9*, 430. [CrossRef]
3. Devries, P.M.R.; Viégas, F.; Wattenberg, M.; Meade, B.J. Deep learning of aftershock patterns following large earthquakes. *Nature* **2018**, *560*, 632–634. [CrossRef] [PubMed]
4. Gardner, J.K.; Knopoff, L. Is the sequence of earthquakes in Southern California, with aftershocks removed, Poissonian? *Bull. Seismol. Soc. Am.* **1974**, *64*, 1363–1367. [CrossRef]
5. Taroni, M.; Akinci, A. Good practices in PSHA: Declustering, b-value estimation, foreshocks and aftershocks inclusion; A case study in Italy. *Geophys. J. Int.* **2021**, *224*, 1174–1187. [CrossRef]
6. Shilen, S.; Toksoz, M.N. A statistical method of identifying dependent events and earthquake aftershocks. *Seismol. Res. Lett.* **1974**, *45*, 3–16. [CrossRef]
7. Sheng, J.Q.; Ma, Q.H.; Ren, X.M.; Zhao, W.M. Aftershock deletion method based on comparison of regional seismic activity frequency. *Earthquake* **2007**, *27*, 85–94.
8. Chen, L.; Liu, J.; Chen, Y.; Chen, L.S. Deletion of aftershocks in seismic activity analysis. *Chin. J. Geophys.* **1998**, *41* (Suppl. 1), 244–252. (In Chinese)
9. Knopoff, L.; Gardner, J.K. Higher seismic activity during local night on the raw worldwide earthquake catalogue. *Geophys. J. Int.* **1972**, *3*, 3. [CrossRef]
10. Shlien, S. A clustering model for earthquake occurrences. *Bull. Seismol. Soc. Am.* **1970**, *60*, 1765–1787.
11. Console, R.; Gasparini, C.; Simoni, B.D.; Marcelli, L.; Vecchi, M. Preambolo al catalogo sismico nazionale (csn). i criteri di informazione del catalogo sismico nazionale (csn). *Ann. Geophys.* **1979**, *32*, 37–77. [CrossRef]
12. Keilis-Borok, V.I.; Knopoff, L.; Rotvain, I.M. Bursts of aftershocks, long-term precursors of strong earthquakes. *Nature* **1980**, *283*, 259–263. [CrossRef]
13. Davis, S.D.; Cliff, F. Single-link cluster analysis, synthetic earthquake catalogues, and aftershock identification. *Geophys. J. Int.* **1991**, *2*, 289–306. [CrossRef]
14. Zhuang, J.; Ogata, Y.; Vere-Jones, D. Stochastic declustering of space-time earthquake occurrences. *J. Am. Stat. Assoc.* **2002**, *97*, 369–380. [CrossRef]

15. Zaliapin, I.; Ben-Zion, Y. Earthquake clusters in southern California I: Identification and stability. *J. Geophys. Res. Solid Earth.* **2013**, *118*, 2847–2864. [CrossRef]
16. Zaliapin, I.; Ben-Zion, Y. Earthquake declustering using the nearest-neighbor approach in space-time-magnitude domain. *J. Geophys. Res. Solid Earth.* **2020**, *125*, e2018JB017120. [CrossRef]
17. Zaliapin, I.; Ben-Zion, Y. Perspectives on clustering and declustering of earthquakes. *Seismol. Res. Lett.* **2022**, *93*, 386–401. [CrossRef]
18. Rosson, Z.; Walter, J.I.; Goebel, T.; Chen, X. Narrow spatial aftershock zones for induced earthquake sequences in Oklahoma. *Geophys. Res. Lett.* **2019**, *46*, 10358–10366. [CrossRef]
19. Baiesi, M.; Paczuski, M. Scale-free networks of earthquakes and aftershocks. *Phys. Rev. E—Stat. Phys. Plasmas Fluids Relat. Interdiscip. Top.* **2004**, *69*, 8. [CrossRef]
20. Dascher-Cousineau, K.; Brodsky, E.E.; Lay, T.; Goebel, T. What controls variations in aftershock productivity? *J. Geophys. Res. Solid Earth.* **2020**, *125*, e2019JB018111. [CrossRef]
21. Zhan, Z.; Jin, B.; Wei, S.; Graves, R.W. Coulomb stress change sensitivity due to variability in mainshock source models and receiving fault parameters: A case study of the 2010–2011 Christchurch, New Zealand, earthquakes. *Seismol. Res. Lett.* **2011**, *82*, 800–814. [CrossRef]
22. Sboras, S.; Lazos, I.; Mouzakiotis, E.; Karastathis, V.; Pavlides, S.; Chatzipetros, A. Fault modelling, seismic sequence evolution and stress transfer scenarios for the July 20, 2017 (MW 6.6) Kos–Gökova Gulf earthquake, SE Aegean. *Acta Geophys.* **2020**, *68*, 1245–1261. [CrossRef]
23. Laurenti, L.; Tinti, E.; Galasso, F.; Franco, L.; Marone, C. Deep learning for laboratory earthquake prediction and autoregressive forecasting of fault zone stress. *Earth Planet Sci. Lett.* **2022**, *598*, 117825. [CrossRef]
24. Lazos, I.; Pikridas, C.; Chatzipetros, A.; Pavlides, S. Determination of local active tectonics regime in central and northern Greece, using primary geodetic data. *Appl. Geomat.* **2021**, *13* (Suppl. 1), 3–17. [CrossRef]
25. Guo, Z.J.; Qin, B.Y.; Xu, W.Y.; Tang, Q. Preliminary study on a model for the development of the focus of an earthquake. *Chin. J. Geophys.* **1973**, *16*, 43–48.
26. Wells, D.; Coppersmith, K. New Empirical Relationships among Magnitude, Rupture Length, Rupture Width, Rupture Area, and Surface Displacement. *Bull. Seismol. Soc. Am.* **1994**, *84*, 974–1002.
27. Deng, Q.D.; Zhang, P.Z.; Ran, Y.K.; Yang, X.P.; Min, W.; Chen, L.C. Active tectonics and earthquake activities in China. *Earth Sci. Front.* **2003**, *10* (Suppl. 1), 66–73.
28. Chen, J.; Li, T.; Sun, J.B.; Fang, J.H.; Yao, Y.; Li, Y.H.; Wang, H.R.; Fu, B. Coseismic surface ruptures and seismogenic Muji fault of the 25 November 2016 Arketao Mw6. 6 earthquake in northern Pamir. *Seismol. Geol.* **2016**, *38*, 1160–1174.
29. Zhou, H.L. Source mechanism of earthquake (Nov.5, 1988) located between Xiji and Totohe Bark in Qinghai Province. *Earthq. Res. China.* **1995**, *11*, 84–91. (In Chinese)
30. Li, Z.H.; Ma, H.S.; Qu, Y.J. Study on seismogenic structure and seismic activity characteristics before the Yutian M7.3 earthquake on March 21, 2008, Xinjiang. *Earthq. Res. China.* **2009**, *25*, 199–205. (In Chinese)
31. Xu, P.S.; Liu, Z.F.; Zhang, Z.Q.; Li, J.; Liu, L.F.; Su, Y.J. Double difference relocation and focal mechanisms of the Jinggu *Ms*6.6 earthquakes sequences in Yunnan Province in 2014. *Earth Sci.—J. China Univ. Geosci.* **2015**, *40*, 1741–1754. (In Chinese)
32. Wei, W.; Xie, C.; Zhou, B.; Zhi, G.; Wang, Y. Location of the mainshock and aftershock sequences of the M6.9 Mainling earthquake, Tibet. *Chin. Sci. Bull.* **2018**, *63*, 1493–1501. (In Chinese) [CrossRef]
33. Luo, F.Z.; Qu, Y.J.; Wang, J. Study on the M7.1 earthquake at the mouth of Kalakunlun MT. in Hetian, Xinjiang on Nov.19, 1996. *Inland Earthq.* **2003**, *17*, 33–38. (In Chinese)
34. Wu, W.W.; Wei, Y.L.; Long, F.; Liang, M.J.; Chen, X.F.; Sun, W.; Zhao, J. Study on source parameters of the 8 August 2017 M7.0 Jiuzhaigou earthquake and its aftershocks, Northern Sichuan. *Seismol. Geol.* **2020**, *42*, 492–512.
35. Shao, Z.G.; Ma, H.S.; Zhang, L.P.; Huang, J.P.; Wen, X.Z. The characteristics of co-seismic slip and aftershocks distribution of the *Ms*7.1 earthquake at Qinghai Yushu in 2010 and its relationship with tectonics. *Chin. J. Geophys.* **2013**, *56*, 3800–3810. (In Chinese)
36. Lei, J.; Zhao, D. Structural heterogeneity of the Longmenshan fault zone and the mechanism of the 2008 Wenchuan earthquake (*Ms*8.0). *Geochem. Geophys. Geosyst.* **2009**, *10*. [CrossRef]
37. Klimenko, M.V.; Klimenko, V.V.; Zakharenkova, I.E.; Pulinets, S.A.; Zhao, B.; Tsidilina, M.N. Formation mechanism of great positive TEC disturbances prior to Wenchuan earthquake on May 12, 2008. *Adv. Space Res.* **2011**, *48*, 488–499. [CrossRef]
38. Chen, M. Aftershocks and Background Seismicity in Tangshan and the Rest of North China. *J. Geophys. Res. Solid Earth* **2021**, *126*, e2020JB021395. [CrossRef]